American Mineralogist, Volume 76, pages 628–640, 1991

Smectite-to-chlorite transformation in thermally metamorphosed volcanoclastic rocks in the Kamikita area, northern Honshu, Japan

ATSUYUKI INOUE
Geological Institute, College of Arts and Sciences, Chiba University, Chiba 260, Japan
MINORU UTADA
The University Museum, University of Tokyo, Tokyo 113, Japan

ABSTRACT

Miocene volcanoclastic rocks at Kamikita, northern Honshu, Japan, exhibit the effects of an intensive episode of thermal metamorphism caused by a hornblende quartz diorite intrusion. Metamorphic zones with a total thickness of approximately 6 km are concentrically developed around the diorite mass. The zones are defined by the sequential appearance of characteristic mineral assemblages from smectite (Zone I), to smectite + heulandite + stilbite (Zone II), to corrensite + laumontite (Zone III), to chlorite + epidote (Zone IV), and finally to biotite + actinolite (Zone V) with increasing metamorphic grade. As smectite transforms to chlorite, the percentage of smectite layers in interstratified chlorite/smectite (C/S) (the intermediate products) decreases discontinuously with increasing metamorphic grades, with steps at 100–80%, 50–40% (corrensite), and 10–0%. The transformation of smectite to chlorite through corrensite is characterized chemically by decreases in Ca and Si, an increase in Al, and a constant Fe/(Fe + Mg) ratio. The mineral paragenesis, structural variation, and compositions all support the hypothesis that corrensite is a thermodynamically stable C/S phase. Corrensite formed at temperatures between approximately 100 and 200 °C. The Kamikita metamorphic zonation was developed in response to a thermal gradient of approximately 70 °C/km, and the secondary minerals crystallized with near-equilibrium compositions.

INTRODUCTION

Mafic phyllosilicates such as saponite, interstratified chlorite/smectite (C/S), and chlorite are abundant in low-grade metabasites. The presence of these minerals has been reported from diagenetic environments (Hoffman and Hower, 1979; Chang et al., 1986), active and fossil geothermal systems (Tomasson and Kristmannsdottir, 1972; Kristmannsdottir, 1983; Inoue et al., 1984a, 1984b; Inoue, 1987; Liou et al., 1985), ophiolites (Evarts and Schiffman, 1983; Bettison and Schiffman, 1988), and oceanic crust (Alt et al., 1986). Interstratified C/S generally occurs as an intermediate product during the smectite-to-chlorite transformation. It is interesting that the nature of interlayering in C/S is temperature sensitive in a fashion similar to illite/smectite (I/S) (e.g., Hoffman and Hower, 1979; Środoń and Eberl, 1984; Horton, 1985). Earlier work reported, for the process of transformation of smectite to chlorite, that the expandability of smectite decreased discontinuously with increasing temperature in diagenetic environments and hydrothermal systems (Inoue et al., 1984a, 1984b; Inoue, 1987). Only a few types of ordered structures, Reichweite = 0 and 1, appeared in intermediate C/S products (Reynolds, 1988). However, Chang et al. (1986) and Schultz (1963) indicated that the expandability of C/S could decrease continuously in limited portions of the entire range of the smectite-to-chlorite transformation, e.g., from smectite to corrensite or from corrensite to smectite. Furthermore, Helmold and van der Kamp (1984) noted that there is a continuous decrease in expandability over the entire range of proportion of smectite layers (%smectite) in C/S. Phase relations of C/S were discussed by Peterson (1961) and Velde (1977). They inferred, on the basis of the phase rule, that C/S is a stable phase.

In this study, we describe the relations for the mafic phyllosilicates from thermally metamorphosed volcanoclastic rocks peripheral to diorite intrusive masses at Kamikita, northern Honshu, Japan. Detailed X-ray powder diffraction and microprobe analyses have been performed on the phyllosilicates and associated calcium aluminum silicate minerals. The objectives of this paper are to clarify the transformation process of smectite to chlorite in the thermal metamorphic environment and the thermodynamic status of corrensite as an intermediate product.

GEOLOGICAL SETTING

The Kamikita area is located in the northern part of Honshu, Japan. As shown in Figure 1, Miocene and Quaternary sequences occur, as does the Kamikita Kuroko-type ore deposit. The geology of the area has been described in detail by many researchers (Miyajima and

0003–004X/91/0304–0628$02.00

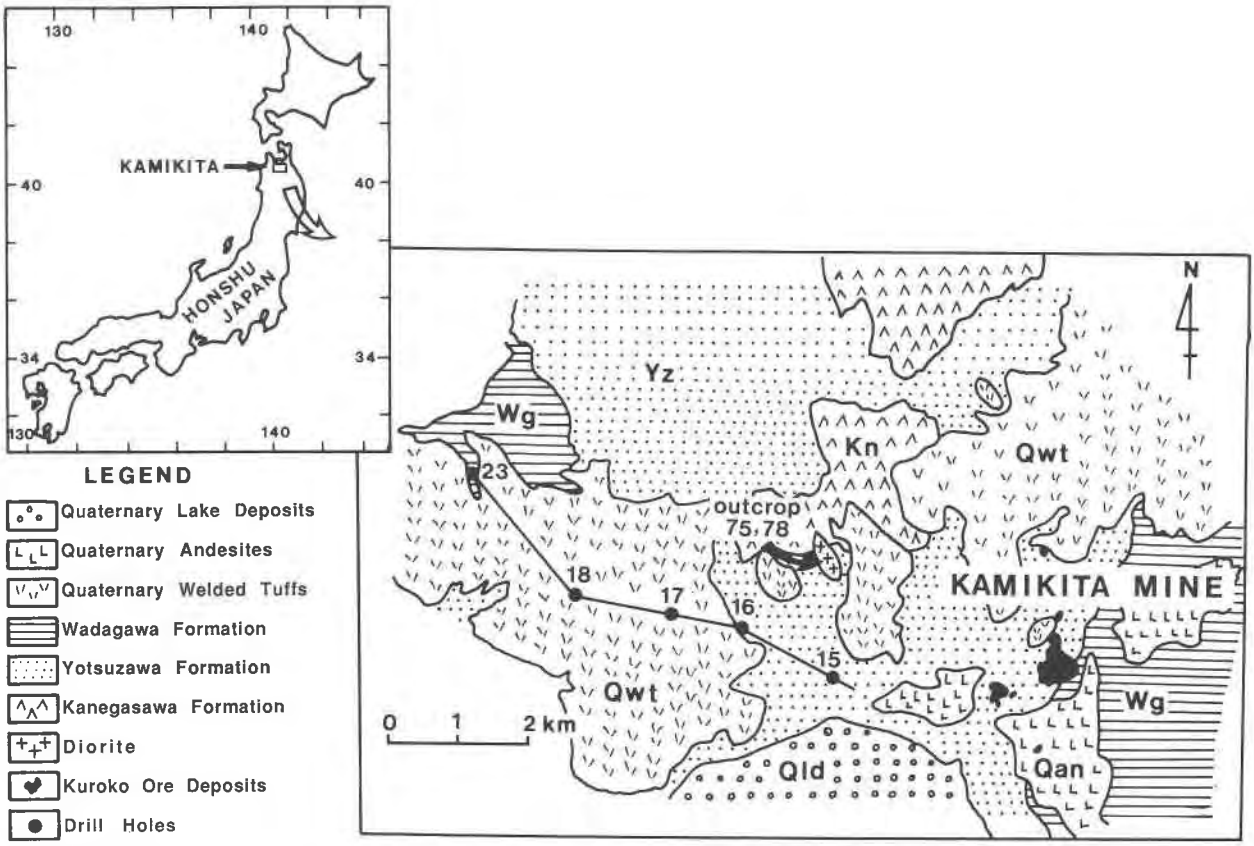

Fig. 1. Geologic map of the Kamikita area indicating localities of drill holes and outcrop samples used in this study.

Mizumoto, 1965, 1968; Lee, 1970; Lee et al., 1974; MMAJ, 1974, 1975, 1986).

The Miocene group consists of three formations in order of decreasing age, as follows: the Kanegasawa formation is composed of massive or brecciated basaltic to andesitic lava flows. The Yotsuzawa formation is composed principally of andesitic to dacitic lava flows and volcanoclastic rocks and some mudstone layers. The Wadagawa formation is composed of felsic and basaltic volcanics. It contains intercalated marine mudstones. The Kamikita Kuroko deposit occurs in the lowermost horizon. Several small diorite bodies have intruded the Kanegasawa and Yotsuzawa formations but hornfelsic rocks are not observed in the field. The Kanegasawa, Yotsuzawa, and Wadagawa formations dip moderately (10–30°) on both sides of an anticlinorium, which has a north-south direction in the study area.

The Quaternary group is divided into three formations: Tashirodai welded tuffs, andesite lava flows, and lake deposits. They unconformably overlie the Miocene sediments and dip gently (0–10°).

A simplified geologic map with the locations of the drill holes utilized in this study is shown as Figure 1, and a geologic cross section including the drill holes is given as Figure 2. A diorite intrusive mass is found at a depth below 400 m of drill hole no. 15, as shown in Figure 2.

Methods

More than 200 samples were collected from outcrops and five drill holes. X-ray powder diffraction (XRD) and thin section studies were used to determine the distribution and textural variation of secondary minerals. The clay size fraction (<1 μm) was obtained by ultrasonic disaggregation and centrifugation of clay-H_2O suspensions. Oriented specimens with an approximate area of 20 × 15 mm were prepared by placing the suspensions on a glass slide. XRD patterns of the air-dried and ethylene-glycol-saturated specimens were obtained using a Rigaku RAD I-B diffractometer (40 kV, 20 mA) equipped with a Cu tube, graphite-monochrometer, and 0.5° divergence and scattering slits. Percentage of smectite layers (%S) and ordering type (Reichweite) of interstratified C/S and I/S were determined by comparing the observed XRD patterns with computer-simulated patterns using the program Newmod (developed by R. C. Reynolds, Dartmouth College, Hanover). XRD patterns of randomly oriented specimens were also obtained in order to determine the $d(060)$ value of mafic phyllosilicates.

Energy-dispersive microprobe analyses of phyllosilicates and calcium-aluminum silicates in polished thin section were conducted on a Hitachi S-550 scanning electron microscope fitted with a Kevex 7000 A-75 solid state

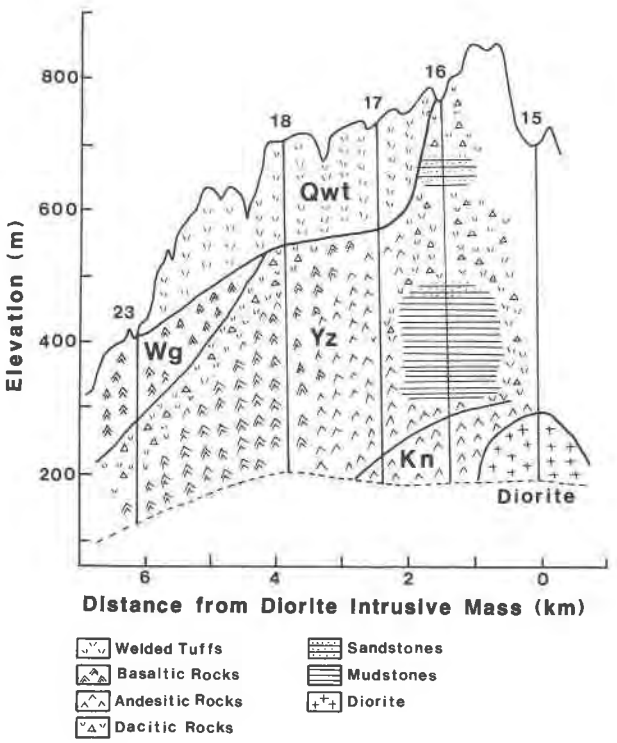

Fig. 2. Geologic cross section along the line of Figure 1. Qwt = Quaternary welded tuffs; Wg = Wadagawa formation; Yz = Yotsuzawa formation; Kn = Kanegasawa formation.

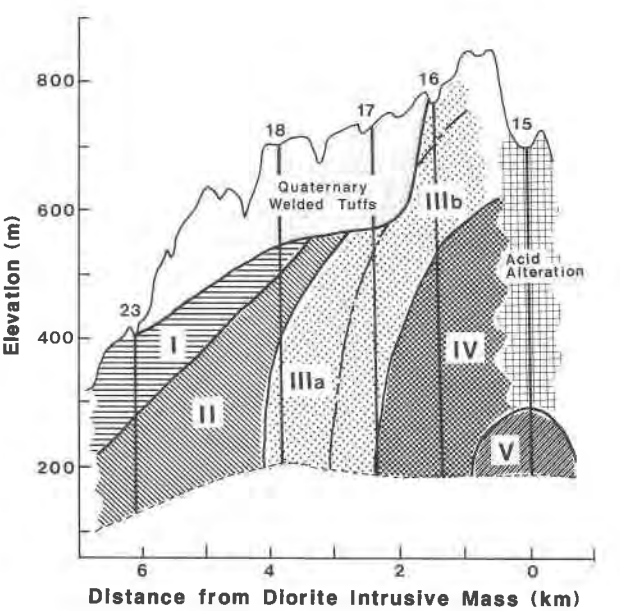

Fig. 3. Cross section showing the distribution of zones.

Table 1. Secondary minerals occurring in zones

Secondary minerals	Zones					
	Zone I	Zone II	Sub-zone IIIa	Sub-zone IIIb	Zone IV	Zone V
α-cristobalite	+					
Quartz	+	+	+	+	+	+
Montmorillonite	+	+				
Saponite	+	+				
Illite/smectite				+		
Corrensite			+	+		
Phengite					+	
Chlorite				+	+	+
Biotite						+
Mordenite		+				
Heulandite		+				
Stilbite		+				
Chabazite		+				
Laumontite			+	+		
Wairakite					+	
Albite			+	+	+	+
Sphene				+	+	
Epidote				+	+	+
Actinolite						+
Calcite	+	+	+	+	+	
Hematite		+	+	+	+	+
Pyrite						+

Note: Zone I = smectite zone, Zone II = smectite-zeolite zone, Subzones IIIa and IIIb = corrensite-laumontite zone, Zone IV = chlorite-epidote zone, Zone V = biotite-actinolite zone.

detector. Analyses were carried out using an accelerating voltage of 20 kV, a beam current of 200 pA, a beam diameter of 2 μm, and a counting time of 200 s. Analyses were obtained on 3–15 points of each mineral in a thin section. EDS data were reduced by a ZAF scheme (QANTX software) which was modified by Mori and Kanehira (1984). The standards included quartz (Si), corundum (Al), periclase (Mg), metals (Fe, Ti, and Mn), calcite (Ca), albite (Na), and potassium chromate crystals (K) (Mori and Kanehira, 1984). The bulk composition of rocks was determined with a JEOL JSX-60PX X-ray fluorescence spectrometer using fused glass disks.

Rock alteration

Six mineralogical zones were defined on the basis of the assemblages of 22 secondary minerals identified in the drill cores, as listed in Table 1. These zones are distributed from the contact of the diorite mass to a distance of approximately 6 km, as shown in Figure 3. The petrographic relations of each zone are described briefly below.

Zone I is defined by the presence of smectite and the absence of other secondary minerals, except calcite and silica minerals. The rocks from the Wadagawa formation and the upper-most part of the Yotsuzawa formation belong to this zone. Brown-colored saponite is common in mafic to intermediate rocks, whereas montmorillonite occurs in felsic rocks. Saponite usually occurs as a replacement of primary orthopyroxene phenocrysts and glassy groundmass in mafic rocks. Montmorillonite principally replaces the glassy groundmass of felsic rocks. Clinopyroxene and plagioclase phenocrysts are unaltered in both rock types except for occasional replacement by saponite

and calcite, respectively. Cristobalite is associated with smectite in the part of this zone of lowest grade, whereas secondary quartz occurs in the part with higher grade.

Zone II is defined by the presence of both smectite and zeolites. The rocks from the upper part of the Yotsuzawa formation belong to this zone. The mode of occurrence of smectite in this zone is the same as that of Zone 1. That is, saponite is a common variety of smectite in mafic to intermediate rocks, and montmorillonite is a common variety in felsic rocks. Where both saponite and montmorillonite were identified (in the upper part of drill hole no. 18) by XRD, each was observed to replace only one kind of rock fragment, as observed in thin section. Stilbite, heulandite, and chabazite occur in mafic rocks; mordenite is dominant in felsic rocks. These zeolites replace glassy groundmass and fill cavities. Weakly albitized plagioclase is partially replaced by calcite or saponite. Secondary quartz occurs as fine-grained aggregates with smectite in the glassy groundmass. Celadonite and vermiculite, which were clearly distinguished from saponite by optical, microprobe, and XRD analyses, were recognized as vesicle fillings in sample 18-320-m, which was located near the boundary between Zones II and III. A precipitation sequence was observed within vesicles from the wall to the center as follows: (1) a transparent thin rim consisting of fine-grained zeolite, quartz, or both (2) fine-grained brown vermiculite, (3) fine-grained bluish-green celadonite, (4) flaky vermiculite and zeolites. The last assemblage is absent in small vesicles.

Zone III is defined by the presence of corrensite and laumontite. The rocks from the middle part of the Yotsuzawa formation belong to this zone. Corrensite generally occurs as a replacement of mafic phenocrysts and glassy groundmass, and as a pore filling identical in mode of occurrence to that of saponite in Zones I and II. It also occurs as inclusions within albitized plagioclase phenocrysts, associated with micaceous clays. Flakes of corrensite are generally less than 0.1 mm in length and show pleochroism from green to pale green. In higher grade parts of the Zone III, however, corrensite is deeper in color and grains are larger. Such corrensite often coexists with spherulites of fine-grained sphene and epidote that are less than 0.1 mm in diameter. Zone III is further divided into two subzones: subzone IIIa (epidote-absent subzone) and subzone IIIb (epidote-present subzone). Laumontite with corrensite occurs commonly in both subzones as pore fillings. Interstratified I/S having $<15\%$ smectite is present in mudstones and sandstones in subzone IIIb.

Zone IV is defined by the general presence of chlorite and epidote and the absence of corrensite and laumontite. The rocks from the lower part of the Yotsuzawa formation and the upper part of the Kanegasawa formation belong to this zone. Chlorite occurs as a replacement of mafic phenocrysts and glassy groundmass, and as a pore filling. It shows strong pleochroism from dark green to pale green. It is also characterized by isotropic-anomalous blue interference colors and both negative and positive elongations. Grains of epidote in this zone are less than 0.3 mm in length but are larger than those found in subzone IIIb. Plagioclase phenocrysts are almost completely replaced by calcite or epidote or both. The remaining plagioclase is strongly albitized. In felsic rocks, phengitic mica coexists with chlorite. Mudstones of this zone are usually composed of illite, chlorite, and quartz. A wairakite-like mineral was occasionally identified in tuffaceous mudstones (samples 16-280-m and 16-300-m). A mudstone sample (16-560-m) is composed of regularly interstratified I/S (rectorite) with hematite and very small amounts of illite, chlorite, and quartz. Veinlets composed of epidote, andradite, and anhydrite are found in an andesite sample (16-576-m).

Zone V is defined by the presence of biotite and actinolite. This zone is recognized only within the diorite mass. Primary hornblende is replaced by fine-grained biotite, actinolite, chlorite, hematite, and pyrite. These secondary minerals have crystallized along the cleavages of hornblende grains. Biotite usually shows strong pleochroism from reddish brown to yellow. In the upper parts of the diorite mass (413–420 m depths of drill hole no. 15), secondary biotite is further altered to interstratified biotite/vermiculite or vermiculite. In this zone, epidote is sporadically found as fine-grained aggregates, and chlorite is characterized by anomalous brown interference colors and negative elongation. Although hematite is commonly found in the rocks of Zones II–V, pyrite is rare in the other zones.

As already reported by Inoue and Utada (1989), dickite, pyrophyllite, zunyite, topaz, alunite, rectorite, sudoite, and tosudite are recognized in the upper parts of drill hole no. 15 above the diorite mass. They are probably the products of an acidic hydrothermal alteration that prevailed at a late stage. The original metamorphic minerals and textures of the rocks in the upper parts of drill hole no. 15 were completely destroyed by the superimposed effects of the acidic hydrothermal alteration.

Structural variation of interstratified clay minerals

Structural variation of interstratified minerals can be clarified by examining changes in position and intensity of the 00l reflections (Reynolds, 1980). Figure 4a shows representative XRD patterns of samples from the saponite-corrensite-chlorite series from the study area. Saponite is recognized by the expansion of the 001 spacing from 14 to approximately 17 Å upon ethylene glycol saturation. The $d(060)$ value is 1.532–1.535 Å (Fig. 4b). Corrensite shows expansion from 29 to 31 Å with ethylene glycol saturation. The value of $d(060)$ of corrensite ranges from 1.540 to 1.542 Å. Chlorite generally has $d(001) = 14.2$ Å and $d(060) = 1.541$–1.545 Å. The value of $d(001)$ does not change with ethylene glycol saturation. XRD patterns of examination, some of the C/S contained broad peaks with intermediate $d(001)$ values of approximately 16.5 Å or 15.1 Å, corresponding to a value be-

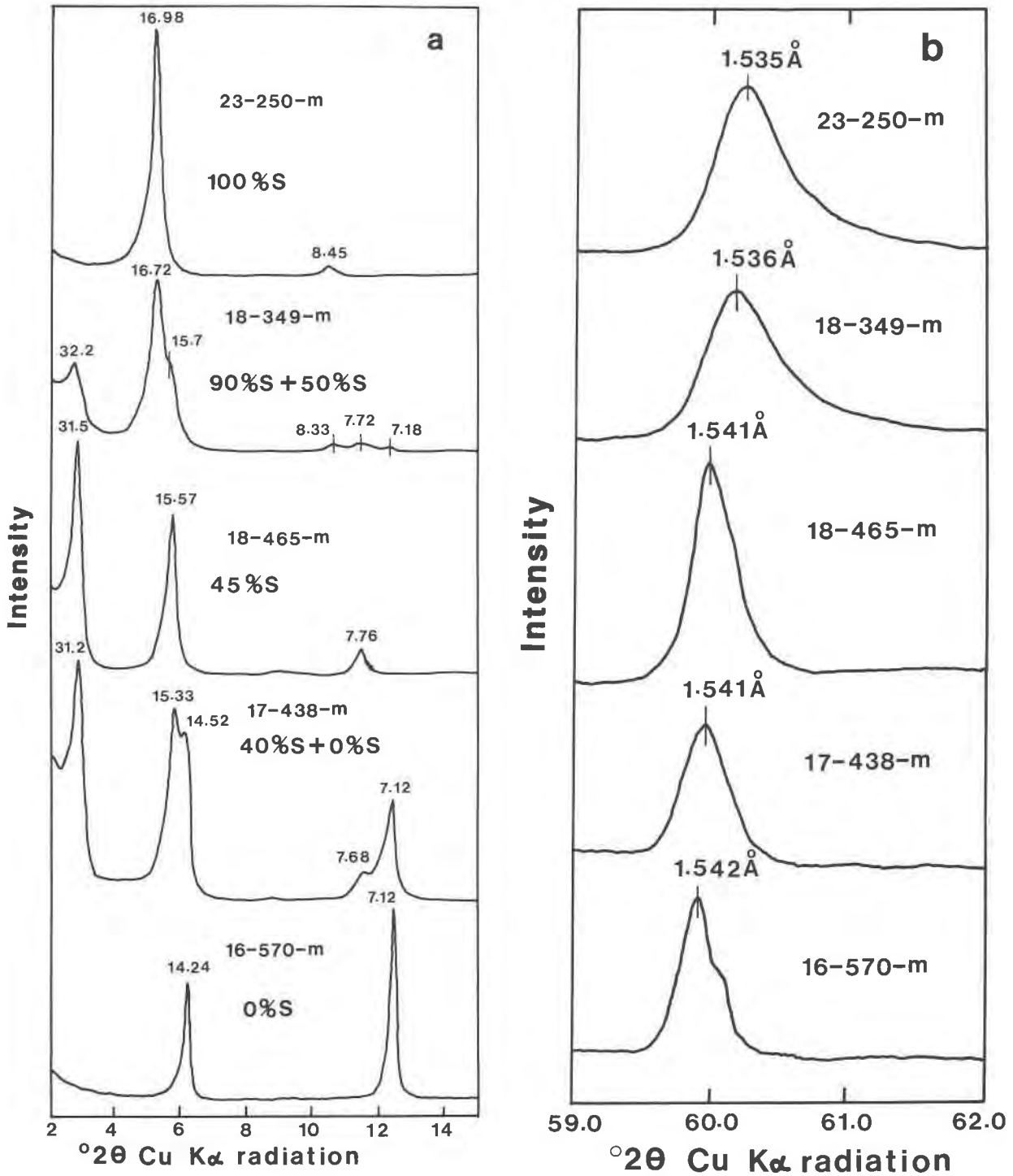

Fig. 4. (**a**) X-ray powder diffraction patterns of samples of the saponite-corrensite-chlorite series. They were recorded on oriented, ethylene-glycol-saturated specimens using step-scanning. The d values of peaks are given in Å. (**b**) The (060) peaks of the same samples as in **a**.

tween those for saponite and corrensite or between those for corrensite and chlorite. The intensities of the reflection with $d = 31$ Å were variable. The relative intensities of the 14-, 7-, and 4.7-Å reflections were intermediate to those of the above two pairs of minerals. Recording of the XRD patterns by means of a step-scanning method revealed that the intermediate $d(001)$ value and intensities were not due to some specific interlayering in C/S but

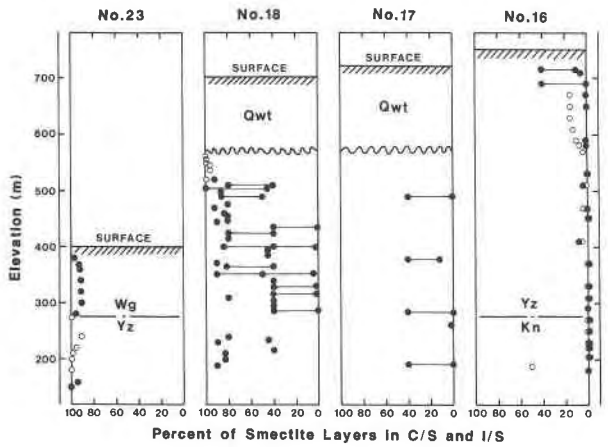

Fig. 5. Variations of percentages of smectite layers in chlorite/smectite (solid circles) and illite/smectite (open circles) as a function of depth of drill holes. The tie lines indicate the presence of more than two chlorite/smectite samples having different smectite layer percentages in a rock specimen. Abbreviations as in Figure 2.

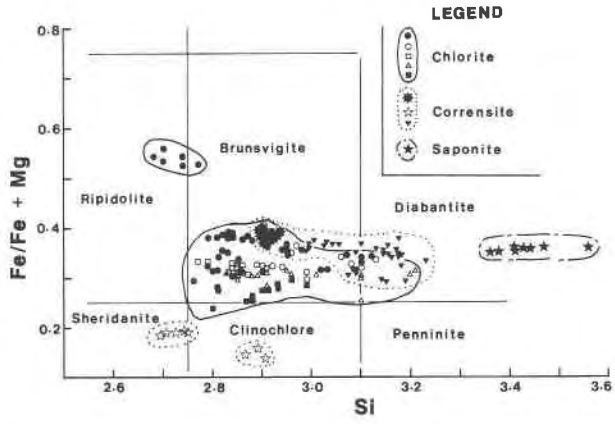

Fig. 6. Compositions of chlorite, corrensite, and saponite from various drill holes. Solid circles and asterisks = drill hole no. 16; open circles and stars = drill hole no. 17; open triangles = drill hole no. 15; solid stars and triangles = drill hole no. 18; open boxes and solid boxes = outcrop samples.

were caused by more than two phases, as clearly illustrated by Figure 4a.

The variation of the relative amount of smectite in C/S and in I/S is illustrated in Figure 5 as a function of depth. The value of %smectite in C/S decreases discontinuously from 100% smectite (saponite) to 0% smectite (chlorite) with intermediate values of 50–40% smectite (corrensite) with increasing metamorphic grade. The % smectite value in saponite is $\geq 80\%$, whereas that in chlorite is $\leq 10\%$. The existence of C/S having intermediate % smectite values other than 50–40% smectite is not certain in the Kamikita area. The intimate association of saponite, corrensite, or chlorite as separate phases is implied by XRD data in samples of drill hole nos. 16, 17, and 18. The C/S having 50–40% smectite (termed corrensite in this study), which yields a superlattice reflection with $d = 31$ Å after ethylene glycol saturation, has a Reichweite (R) value of 1. The C/S that is more or less expandable than corrensite may have $R = 0$. The C/S in drill hole no. 18 shows irregular variation in the proportion of smectite with depth. These data imply that less expandable C/S occurs commonly in porous rocks like tuffaceous breccias and hyaloclastites, and more expandable C/S dominates in massive rocks like lavas.

The variation of proportion of smectite in I/S shown in Figure 5 varies discontinuously. The I/S from core nos. 18 and 23 generally is pure smectite. The I/S in mudstones and sandstones in the upper part of core no. 16 (near the lower end of subzone IIIa) contains 15% smectite (Fig. 5) and the I/S has $R = 3$ ordering. The proportion of smectite in I/S decreases continuously from 15 to 0% with depth in drill hole no. 16. The proportion of smectite layers in I/S is zero approximately where corrensite no longer occurs. The trends in variation of proportion of smectite in I/S at intermediate I/S values is not clearly defined in the Kamikita area because dioctahedral clays are rare in core nos. 17 and 18.

Variations in composition of secondary minerals

Representative analyses of selected minerals are listed in Tables 2–4. The total Fe for phyllosilicates and actinolite was calculated as Fe^{2+} and as Fe^{3+} for epidote and garnet.

Saponite

The Si content of saponite ranges from 3.36 to 3.56, and the Fe/(Fe + Mg) ratio from 0.351 to 0.361 (Table 2 and Fig. 6). The interlayer cation is principally Ca. The saponite composition ranges are essentially identical for all modes of occurrence.

Corrensite

Empirical formulas of corrensite were normalized to $O_{20}(OH)_{10}$ (Newman and Brown, 1987). The Si content was variable from grain to grain but was relatively constant within a grain. The Fe/(Fe + Mg) ratio ranges from 0.3 to 0.4 (Table 2 and Fig. 6). The corrensite in samples 17-438-m and 17-343-m has ratios less than 0.2, however. The general petrographic characteristics of the latter corrensite samples are nearly the same as those of the others, except that the latter are larger in size and deeper in color.

Figure 7 shows a plot of $^{[4]}Al$, vs. the total number of octahedral cations for corrensite. Inoue (1985) demonstrated that there is a linear relation between those two variables for Fe-rich corrensite ($0.52 < Fe/(Fe + Mg) < 0.61$). This relationship is shown by the solid line in Figure 7. The data for Kamikita corrensite also fall along the line. Ideally, corrensite has nine octahedral ions per

Table 2. Representative analyses of saponite (1), corrensite (2–4), and chlorite (5–11)

Sample	(1) 18-240	(2) 18-360	(3) 18-465	(4) 16-60
SiO_2	44.18	33.27	33.76	31.88
TiO_2	—	—	—	—
Al_2O_3	7.86	13.12	13.10	15.46
FeO*	15.34	16.21	17.77	20.25
MnO	0.08	0.34	0.19	0.08
MgO	15.64	20.71	18.24	17.69
CaO	2.68	0.76	1.12	1.15
Na_2O	—	—	—	—
K_2O	0.30	—	0.08	0.04
Total	85.95	84.40	84.25	86.55
Numbers of O atoms	11	25	25	25
Si	3.43	6.15	6.29	5.87
$^{[4]}$Al	0.57	1.85	1.71	2.13
$^{[4]}$Total	4.00	8.00	8.00	8.00
Ti	—	—	—	—
$^{[6]}$Al	0.15	1.01	1.17	1.23
Fe	1.00	2.51	2.77	3.12
Mn	0.01	0.05	0.03	0.01
Mg	1.81	5.71	5.07	4.86
$^{[6]}$Total	2.97	9.28	9.04	9.22
Ca	0.23	0.15	0.22	0.23
Na	—	—	—	—
K	0.03	—	0.02	0.01
Fe/(Fe + Mg)	0.356	0.305	0.353	0.391
Range in Fe/(Fe + Mg)	0.351–0.361	0.290–0.317	0.341–0.378	0.370–0.398
Range in Si	3.36–3.56	6.15–6.38	6.20–6.36	5.79–5.87
Range in numbers of oct. cations	2.82–3.06	9.01–9.28	8.99–9.16	9.22–9.38

* Total Fe as FeO.

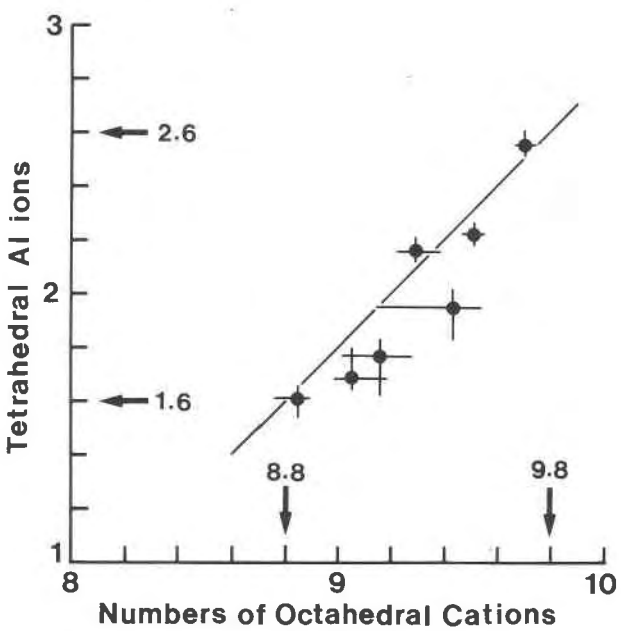

Fig. 7. Plot of $^{[4]}$Al content vs. total of octahedral cations per $O_{20}(OH)_{10}$ in corrensite. Bars indicate ranges of data. The solid line indicates the correlation of Fe-rich corrensite as noted by Inoue (1985).

$O_{20}(OH)_{10}$. The number of octahedral cations ranges from 8.85 to 9.7. These values correspond to 52–38% smectite if the number of octahedral cations is assumed to be six per $O_{20}(OH)_4$ for saponite, nine for corrensite, and 12 per $O_{20}(OH)_{16}$ for chlorite. The proportions of smectite interlayered with corrensite estimated from the chemical composition are consistent with those determined by XRD, as described above. Consequently, if the linear relation of the numbers of octahedral cations vs. the tetrahedral Al content as shown in Figure 6 is a general relation for corrensite, we infer that the C/S, which provided a superlattice reflection at 31 Å after ethylene glycol saturation, contains approximately $Si_{5.4}Al_{2.6}$ – $Si_{6.4}Al_{1.6}$ per $O_{20}(OH)_{10}$ in the tetrahedral sheet and 8.8–9.8 cations in the octahedral sheet. The estimated values are in satisfactory agreement with analyzed values for corrensite from hydrothermal systems (Seki et al., 1983), diagenetic environments (Chang et al., 1986), and ophiolites (Evarts and Schiffman, 1983; Bettison and Schiffman, 1988).

Chlorite

The compositional data for chlorite are plotted in a Foster-type diagram in Figure 6 (Foster, 1962). The number of Si atoms ranges from 2.75 to 3.2, and the Fe/(Fe + Mg) ratio from 0.24 to 0.40. For the chlorite of sample 16-546-m, which filled pore spaces of andesitic volcanics, however, the number of Si atoms ranges from 2.68 to 2.77, and the Fe/(Fe + Mg) ratio ranges from 0.525 to

TABLE 2—*Continued*

(5) 17-459	(6) 16-140	(7) 16-242	(8) 16-480	(9) 16-570	(10) 15-480	(11) outcrop 75
28.26	29.40	27.93	26.96	26.43	27.88	28.90
—	—	—	—	—	0.12	—
16.97	15.65	20.09	20.20	18.87	16.84	17.04
19.40	18.61	19.52	18.01	16.86	17.00	16.00
0.46	0.34	0.40	0.34	0.41	0.59	0.16
20.21	20.35	18.35	19.56	20.75	21.56	22.75
0.14	0.13	0.30	0.15	0.11	0.06	0.11
—	—	—	—	—	0.04	—
0.06	—	—	—	—	0.42	—
85.50	84.48	86.59	85.22	83.43	84.49	84.97
14	14	14	14	14	14	14
2.96	3.10	2.88	2.81	2.81	2.94	2.99
1.04	0.90	1.12	1.19	1.19	1.06	1.01
4.00	4.00	4.00	4.00	4.00	4.00	4.00
—	—	—	—	—	0.01	—
1.06	1.04	1.32	1.29	1.17	1.03	1.07
1.70	1.64	1.68	1.57	1.50	1.50	1.38
0.04	0.03	0.03	0.03	0.04	0.05	0.01
3.16	3.20	2.82	3.04	3.29	3.38	3.50
5.96	5.91	5.85	5.93	6.00	5.97	5.96
0.02	0.01	0.03	0.02	0.01	0.01	0.01
—	—	—	—	—	0.01	—
0.01	—	—	—	—	0.06	—
0.350	0.339	0.373	0.341	0.313	0.307	0.283
0.350–0.399	0.310–0.345	0.364–0.379	0.337–0.350	0.302–0.325	0.299–0.327	0.238–0.296
2.90–2.97	2.90–3.12	2.86–2.91	2.81–2.85	2.79–3.02	2.83–3.10	2.80–2.99
5.96–5.98	5.70–5.92	5.83–5.88	5.93–5.95	5.93–6.04	5.80–6.04	5.96–6.03

0.558. Except for this one specimen, however, the Si content and the Fe/(Fe + Mg) ratio of Kamikita chlorite tend to be smaller with increasing metamorphic grade (Figs. 6 and 8).

TABLE 3. Representative analyses of biotite (1–2) and phengite (3–4)

Sample	(1) 15-440	(2) 15-500	(3) 16-498	(4) 16-520
SiO_2	36.84	38.33	50.38	49.64
TiO_2	4.11	2.62	0.23	0.20
Al_2O_3	12.77	11.42	28.66	27.07
FeO*	11.00	12.02	3.83	5.42
MnO	0.15	0.20	—	—
MgO	17.36	19.46	2.78	3.42
CaO	0.71	0.02	0.13	0.14
K_2O	9.73	8.46	10.24	9.22
Total	92.65	92.52	96.25	95.11
		O = 11		
Si	2.80	2.90	3.34	3.35
$^{[4]}$Al	1.19	1.02	0.66	0.65
Fe	0.01	0.08	—	—
$^{[4]}$Total	4.00	4.00	4.00	4.00
Ti	0.24	0.15	0.01	0.01
$^{[6]}$Al	0.00	0.00	1.58	1.50
Fe	0.69	0.68	0.21	0.31
Mn	0.01	0.01	—	—
Mg	1.97	2.19	0.27	0.34
$^{[6]}$Total	2.91	2.95	2.07	2.16
Ca	0.06	0.00	0.01	0.01
K	0.94	0.82	0.87	0.79
Fe/(Fe + Mg)	0.262	0.258		
Range in Fe/(Fe + Mg)	0.239–0.309	0.222–0.268		
Range in Si	2.80–2.88	2.89–2.98		

* Total Fe as FeO.

Figure 9 is a plot of $^{[4]}Al - 1$ vs. $^{[6]}Al + 2Ti - 1$ for Kamikita chlorite. The 1:1 line in Figure 9 illustrates the Tschermak substitution (Al + Al ≒ Si + Mg). Analyses plotting above the 1:1 line show dioctahedral substitution (Al_2Mg_{-1}) and correspond to octahedral vacancies (Laird, 1988). Analytical data for most chlorite from Zone IV plot above the 1:1 line, suggesting the existence of octahedral vacancies. Data for chlorite in Zone V appears to approach the 1:1 line, implying a smaller proportion of octahedral vacancies. The total Al content also tends to decrease in chlorite from Zone IV to that from Zone V.

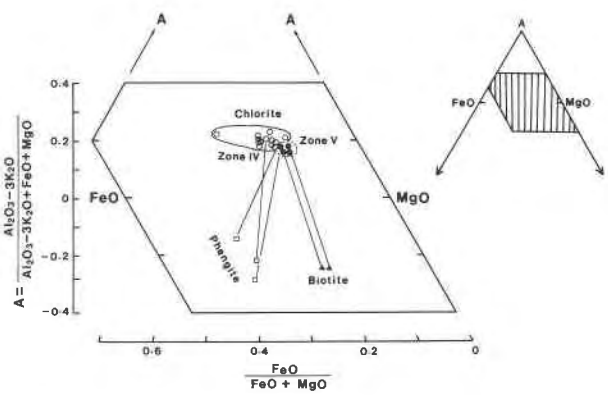

Fig. 8. Compositions of chlorite, phengite, and biotite. Open and solid circles indicate chlorite compositions (averages) from Zones IV and V, respectively. The tie lines correspond to coexisting chlorite and biotite, and chlorite and phengite.

TABLE 4. Representative analyses of epidote (1–6), actinolite (7), andradite (8), heulandite (9), and laumontite (10)

Sample	(1) 17-228	(2) 17-438	(3) 16-498	(4) 16-520	(5) 16-546	(6) 16-570	(7) 15-500	(8) 16-570	(9) 18-231	(10) 18-465
SiO_2	37.41	38.03	37.39	37.36	37.41	37.37	53.30	35.70	58.14	52.27
TiO_2	—	—	0.04	0.24	—	—	—	—	0.07	—
Al_2O_3	24.60	24.68	25.83	23.83	23.24	22.10	1.28	—	17.06	20.82
Fe_2O_3	11.56	11.67	10.51	12.30	13.28	15.16	—	30.82	—	—
FeO	—	—	—	—	—	—	9.11	—	0.49	0.21
MnO	0.30	0.13	0.22	0.14	0.21	0.24	0.88	0.59	—	—
MgO	—	—	—	—	—	—	18.12	—	0.48	—
CaO	23.18	23.42	23.71	23.41	23.35	23.16	10.82	33.20	6.75	10.30
Na_2O	—	—	—	—	—	—	0.25	—	0.72	0.60
K_2O	—	—	—	—	—	—	—	—	1.80	0.36
Total	97.05	97.93	97.70	97.28	97.49	98.03	93.75	100.31	85.51	84.54
Numbers of O atoms	25	25	25	25	25	25	23	12	72	72
Si	5.98	6.01	5.92	5.97	5.99	5.99	7.85	3.01	26.72	24.54
Ti	—	—	0.01	0.03	—	—	—	—	0.04	—
Al	4.63	4.60	4.82	4.49	4.39	4.18	0.22	—	9.24	11.52
Fe^{3+}	1.39	1.39	1.25	1.48	1.60	1.83	—	1.96	—	—
Fe^{2+}	—	—	—	—	—	—	1.12	—	0.16	0.06
Mn	0.04	0.02	0.03	0.02	0.03	0.03	0.11	0.04	—	—
Mg	—	—	—	—	—	—	3.98	—	0.32	—
Ca	3.97	3.97	4.02	4.01	4.01	3.98	1.71	3.00	3.32	5.22
Na	—	—	—	—	—	—	0.07	—	0.64	0.54
K	—	—	—	—	—	—	—	—	1.04	0.24
Total	16.01	15.99	16.03	16.00	16.01	16.01	15.07	8.01	41.52	42.06
X_{ps}	0.23	0.23	0.21	0.25	0.27	0.31				
Range in X_{ps}	0.23–0.27	0.21–0.23	0.21–0.26	0.20–0.29	0.21–0.32	0.22–0.31				

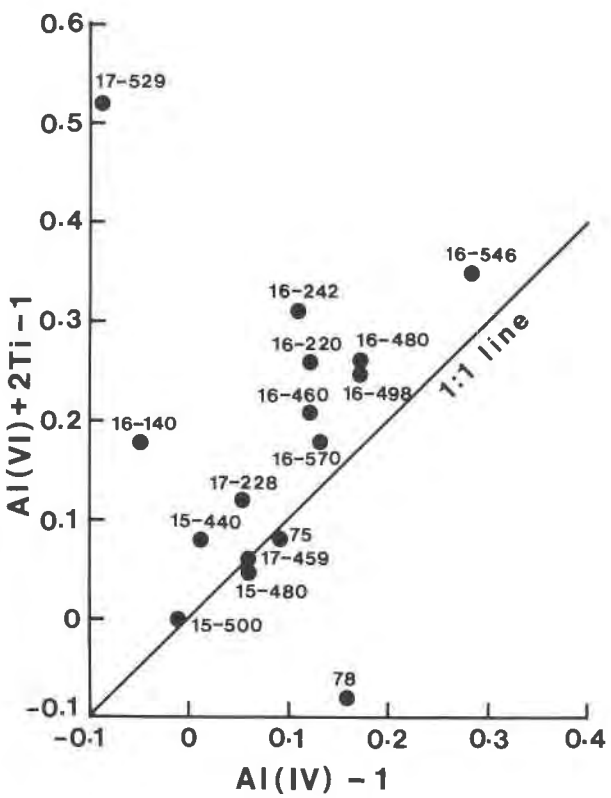

Fig. 9. Plot of $^{[4]}Al - 1$ vs. $^{[6]}Al + 2Ti - 1$ in chlorite. Individual points indicate average compositions of chlorite. The numbers correspond to drill-hole depths of the samples.

Biotite

The brown-colored phyllosilicate present in Zone V shows a wide variation in K content from 0.18 to 0.94 K per $O_{10}(OH)_2$. The low K content corresponds to vermiculitized biotite. The grains with more than 0.7 K are classified as biotite in this study. The Kamikita biotite is characterized by high TiO_2 contents, ranging from 1.96 to 5.31 wt% (3% on average). The average TiO_2 content of vermiculitized biotite is smaller (0.6 wt%). The apparent distribution coefficients of Mg and Fe for biotite and chlorite, K_d = [(Mg/Fe)Bt/(Mg/Fe)Chl], range from 0.99 to 1.15. These values are slightly larger than those reported from rocks of higher metamorphic grade (Ernst et al., 1981; Lang and Rice, 1985; Holdaway et al., 1988).

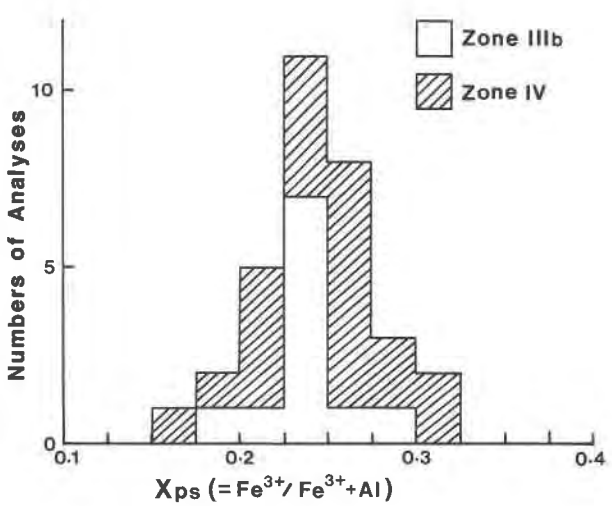

Fig. 10. Distribution of X_{ps} (= $Fe^{3+}/Fe^{3+} + Al^{3+}$) in epidote samples from Zones IIIb and IV.

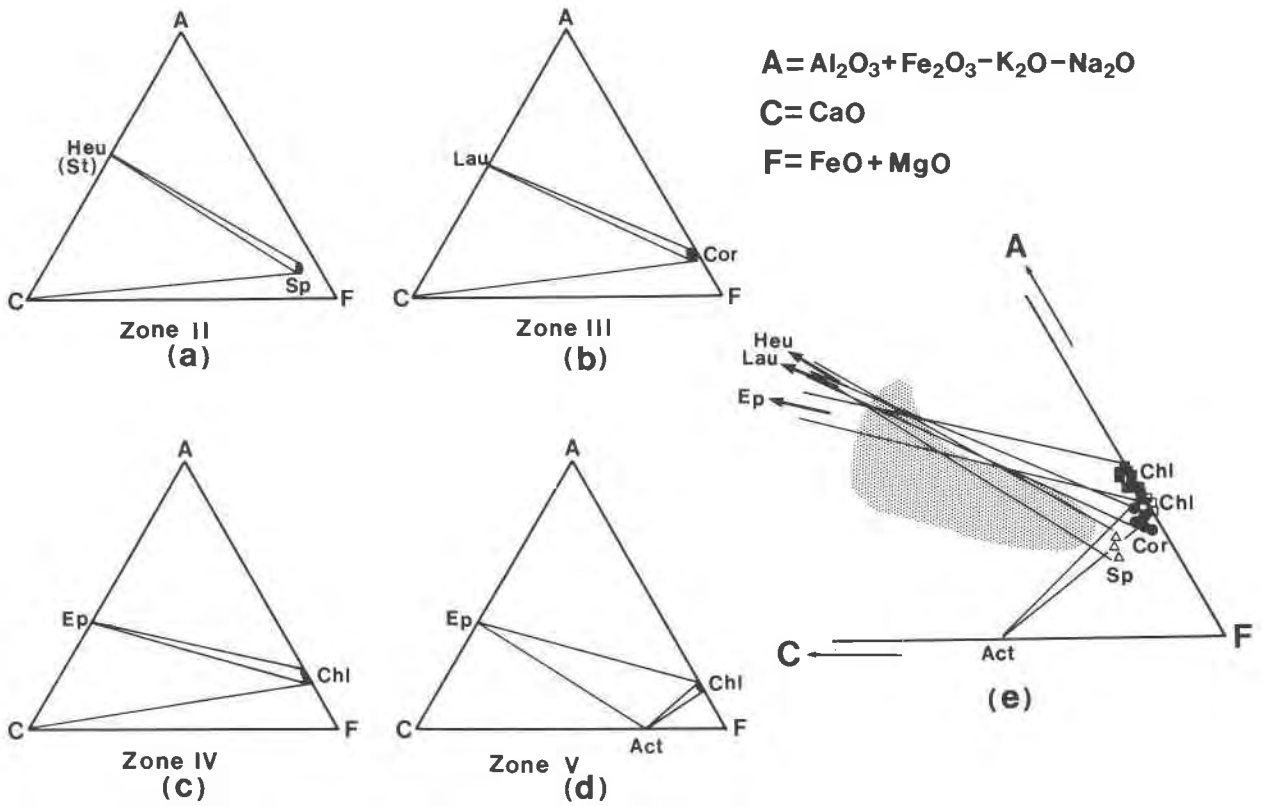

Fig. 11. ACF diagrams illustrating progressive changes in mineral assemblages with increasing metamorphic grade. Heu = heulandite; St = stilbite; Lau = laumontite; Ep = epidote; Act = actinolite; Sp = saponite; Cor = corrensite; Chl = chlorite. (a)–(d) Relations for Zones II, III, IV, and V, respectively. (e) Bulk rock compositions plot within the gray area.

Epidote

The distribution of the pistacite component, $X_{ps} = Fe^{3+}/(Fe^{3+} + Al)$, is given in Figure 10. Epidote grains in Zone IV generally exhibit smaller values of X_{ps} in cores and larger values in rims. Epidote (X_{ps} = 0.22–0.30) associated with andradite in a veinlet of sample 16-576-m is apparently not in equilibrium with the andradite because the andradite contains no Al (Table 4).

Actinolite

The Si content of actinolite ranges from 7.82 to 7.85 per $O_{22}(OH)_2$ and the Al and alkali contents are correspondingly low. The Fe/(Fe + Mg) ratio ranges from 0.215 to 0.219, and the apparent distribution coefficient, K_d = [(Fe/Mg)Chl/(Fe/Mg)Act], = 1.30–1.34.

Other minerals

Analyses of phengite coexisting with chlorite in sandstones and felsic volcanics of Zone IV are given in Table 3 and plotted in Figure 8. Analyses of heulandite and laumontite are given in Table 4.

Progressive phase relations

Phase relations of the mafic phyllosilicates in the Kamikita low-grade metamorphic rocks can be determined by the compositional variations and parageneses of the secondary minerals described above. Textural and chemical equilibria are rarely attained, and only local equilibrium may be realized in low-grade metamorphism (Bishop, 1972; Zen, 1974; Coombs et al., 1976). Although it is not possible to prove that the studied samples formed under equilibrium conditions, the orderly, systematic, and predictable changes in mineral occurrences, as shown in Table 1 and Figure 3, indicate that stable mineral assemblages can be identified.

The inferred stable mineral assemblages within the Kamikita metabasites can be illustrated using ACF diagrams (Fig. 11). The secondary mineral assemblage in basic to intermediate rocks of the lowest grade (Zone I) is saponite + calcite. Primary plagioclase remains almost intact in rocks of Zone I. In Zone II, the secondary mineral assemblage is saponite + heulandite + stilbite + calcite (Fig. 11a). In the higher grade Zone III, this assemblage is replaced by corrensite + laumontite + calcite. In the ACF diagram, the corrensite-laumontite tie line intersects the saponite-heulandite (or stilbite) tie line (Fig. 11e). Tran-

Table 5. Bulk compositions of altered rocks

Sample	SiO_2	TiO_2	Al_2O_3	FeO*	MnO	MgO	CaO	Na_2O	K_2O	P_2O_5	Zone
No. 18											
240	55.42	0.75	15.72	10.04	0.10	7.04	8.75	1.88	0.15	0.15	II
251	55.41	0.81	17.46	8.98	0.08	6.66	8.26	1.78	0.45	0.11	II
308	64.32	1.09	13.94	7.96	0.10	3.35	3.70	4.28	1.10	0.16	IIIa
360	57.01	0.92	16.22	9.42	0.11	5.89	4.64	5.65	0.05	0.09	IIIa
405	58.27	0.74	15.50	10.43	0.13	4.66	3.88	6.14	0.16	0.08	IIIa
420	56.24	0.90	14.96	10.03	0.11	6.62	8.57	2.21	0.25	0.09	IIIa
459	53.02	0.85	15.58	9.61	0.20	7.01	11.44	2.09	0.07	0.12	IIIa
465	60.68	1.10	16.25	7.44	0.09	3.24	3.37	7.64	0.04	0.15	IIIa
480	54.28	0.86	16.23	9.60	0.12	7.05	9.57	1.75	0.43	0.10	IIIa
No. 17											
228	51.90	0.83	17.93	8.96	0.14	6.38	7.59	5.31	0.83	0.13	IIIb
343	51.55	0.89	14.56	9.46	0.11	12.08	6.07	3.88	1.28	0.11	IIIb
438	52.27	1.03	16.23	9.90	0.16	10.82	2.94	5.26	1.27	0.12	IIIb
459	56.29	0.70	18.20	8.52	0.14	4.62	7.05	2.90	1.48	0.10	IIIb
529	54.55	0.81	16.38	9.04	0.13	9.35	4.32	3.98	1.32	0.11	IV
No. 16											
60	52.02	1.02	17.27	10.55	0.04	8.08	9.02	1.82	0.09	0.07	IIIb
140	57.91	0.73	17.78	7.94	0.12	5.81	4.51	2.94	2.19	0.08	IIIb
220	55.67	0.85	16.84	8.99	0.14	7.46	1.48	5.40	1.92	0.10	IIIb
242	54.46	0.94	17.02	10.14	0.17	8.41	3.74	3.17	1.79	0.15	IV
460	54.66	1.08	16.84	10.06	0.14	7.16	5.18	3.10	1.68	0.10	IV
480	64.30	0.76	13.67	7.25	0.12	5.86	1.99	3.29	1.64	0.11	IV
498	75.95	0.17	12.91	1.66	0.05	1.73	1.57	3.28	2.65	0.03	IV
546	58.05	1.08	16.88	10.07	0.19	4.27	3.08	5.60	0.68	0.10	IV
570	54.17	1.03	16.70	10.38	0.18	7.02	7.25	3.13	0.02	0.11	IV
No. 15											
480	63.49	0.82	14.36	7.38	0.20	4.05	5.48	2.68	1.43	0.10	V
500	62.59	0.79	13.98	7.91	0.17	4.03	5.91	2.96	1.58	0.08	V
Outcrop											
78	51.81	0.88	16.59	10.91	0.19	6.26	11.38	1.74	0.15	0.10	V

* Total Fe as FeO.

sition from Zone II to Zone III is marked by transformation of saponite to corrensite; the corrensite has more Al, less Ca and Si, and a nearly constant Fe/(Fe + Mg) ratio as compared to saponite. Heulandite and stilbite were also replaced by laumontite.

The characteristic assemblage of Zone IV is chlorite + epidote + calcite (Fig. 11c). In the transition from Zone III to Zone IV, the chlorite-epidote tie line intersects that of corrensite-laumontite (Fig. 11e). Fe^{3+} is accommodated preferentially in epidote and hematite, and as a result the $Fe^{2+}/(Fe^{2+} + Mg)$ ratios of corrensite and chlorite are equal, as shown in Figure 7. However, since the Al content of chlorite is larger than that of corrensite and epidote contains much more Ca than laumontite, the chlorite-epidote tie line intersects that of corrensite-laumontite. Subzone IIIb may be a transition zone between subzone IIIa and Zone IV because the coexistence of chlorite, corrensite, laumontite, and epidote were demonstrated in subzone IIIb. The bulk compositions of the mafic phyllosilicate-bearing rocks (Table 5) plot near the area where the three tie lines in the ACF diagram intersect each other (Fig. 11e). This implies that the assemblages of secondary minerals changed from Zone II to Zone IV in response to an increase in temperature under nearly isochemical conditions.

The highest grade assemblage is biotite + actinolite + chlorite. Chlorite contains progressively more Mg and less Al as a result of the formation of Mg-rich actinolite and biotite in rocks with scarce epidote and abundant albite.

Discussion

As described above, saponite and chlorite do not show a continuous change in proportion of layers of chlorite during thermal metamorphism in the Kamikita area. Only corrensite having 50–40% smectite layers was formed at intermediate stages of the smectite-to-chlorite transformation. The corrensite coexists with saponite or chlorite or both. Each of these minerals is interpreted to be a distinct, separate phase. Each is quite distinct in chemical composition. The phase relations and structure variations of the smectite-corrensite-chlorite series indicate that corrensite should be regarded as a single interstratified phase from a thermodynamic point of view. This conclusion supports previous inferences concerning thermodynamic relations for corrensite (Peterson, 1961; Velde, 1977; Evarts and Schiffman, 1983; Reynolds, 1988). More recently, Shau et al. (1990) also concluded from their detailed TEM/AEM study of corrensite from the Taiwan ophiolite that corrensite should be treated as a unique phase rather than as a 1:1 ordered mixed-layer C/S.

A discontinuous decrease in proportion of smectite in C/S during the smectite-to-chlorite transformation has been observed in hydrothermal systems and diagenetic environments in previous studies (Inoue et al., 1984a, 1984b; Inoue, 1987), as in the present study. On the other hand, Chang et al. (1986) described a burial sequence with continuous decrease in proportion of smectite layers from saponite to corrensite in Brazilian offshore sedi-

ments. Schultz (1963) noted that C/S could range continuously from 50% smectite to 0% smectite with transformation of smectite to chlorite, although he noted the absence of C/S that contains more than 50% smectite. The detailed examination of XRD patterns of C/S having intermediate $d(001)$ values in this study indicate that they are mixtures of more than two discrete phases. These relations suggest that a discontinuous decrease in proportion of smectite layers in C/S occurs commonly in the entire compositional range of the smectite-to-chlorite transformation.

The physical conditions of corrensite formation and metamorphism in the Kamikita area can be approximated by analogy with observations from hydrothermally altered rocks in geothermal fields. The transition between Zones II and III is characterized by the heulandite- (or stilbite-) laumontite transition as well as by the saponite-to-corrensite transformation. Liou (1971) experimentally determined the maximum temperature of stilbite stability to be 100 °C at 300 bars. Heulandite is structurally similar to stilbite (Gottardi and Gali, 1985). Therefore the boundary between Zones II and III is thought to be at approximately 100 °C in the Kamikita area. The temperature of the first appearance of discrete chlorite with or without C/S has been documented to be 150–240 °C from many geothermal systems (Kristmannsdottir, 1979; McDowell and Elders, 1980, 1983; Keith and Bargar, 1988). Laumontite is present at temperatures below 200 °C and epidote usually occurs at temperatures greater than 200–250 °C in geothermal fields (Bird et al., 1984). The interstratified $R = 3$ I/S near the lower end of subzone IIIa contained 15% smectite and the % smectite in I/S approaches zero in Zone IV. The corresponding temperature is usually 200–230 °C (Środoń and Eberl, 1984). It can reasonably be inferred that the temperature at the boundary between Zones III and IV, where corrensite disappeared, was approximately 200 °C. Accordingly, it is inferred that corrensite occurred at temperatures of approximately 100–200 °C in the Kamikita area. The Kamikita metamorphic zonation (Zones I–IV) was formed in response to a thermal gradient of approximately 70 °C/km and relatively high f_{O_2} conditions, as deduced from the presence of hematite. The diorite mass, Zone V, attained a temperature of approximately 300 °C, as inferred from the temperature of the first appearance of biotite in the Salton Sea geothermal field (Cho et al., 1988). The isolated presence of the epidote + andradite + anhydrite assemblage as a vein in the 16-576-m sample and the presence of pyrite in the diorite mass may suggest local circulation of hydrothermal fluids in a hydrothermal stage following the diorite intrusion.

Summary and conclusions

The results of this study can be summarized as follows:

1. During thermal metamorphism in the Kamikita area, saponite transformed to chlorite through corrensite with increasing metamorphic grade so that the proportion of smectite layers in intermediate C/S decreased discontinuously, with steps at 100–80% (saponite), 50–40% (corrensite), and 10–0% (chlorite). C/S having intermediate % smectite values other than those of the above three ranges was not found. Such a discontinuous transformation of smectite to chlorite is probably a general relation in various geologic environments.
2. The saponite-to-chlorite transformation at Kamikita took place with decreases in Si and Ca, increase in Al, and a nearly constant Fe/(Fe + Mg) ratio. Saponite, corrensite, and chlorite were distinctly different in composition.
3. In addition to the structural and compositional variations in the saponite-corrensite-chlorite series, the mineral paragenesis implies that corrensite should be regarded as a single interstratified phase from a thermodynamic point of view. The formation of C/S having other intermediate % smectite values, except that of corrensite, may be restricted during the smectite-to-chlorite transformation.
4. Corrensite formed at temperatures of approximately 100–200 °C. The formation of corrensite may be facilitated in more permeable rocks, which are more affected by hydrothermal fluids.

Acknowledgments

The authors gratefully thank B. Velde, A. Meunier, and D. Beaufort for their helpful reviews of an initial version of the manuscript. They also acknowledge the help of H. Tatematsu, Japan Railway Research Institute, who supplied the core samples and allowed publication of this study.

References cited

Alt, J.C., Honnorez, J., Laverne, C., and Emmermann, R. (1986) Hydrothermal alteration of a 1 km section through the upper oceanic crust, DSDP Hole 504B: Mineralogy, chemistry, and evolution of seawater-basalt interactions. Journal of Geophysical Research, 91, 10309–10335.

Bettison, L., and Schiffman, P. (1988) Compositional and structural variations of phyllosilicates from the Point Sal ophiolite, California. American Mineralogist, 73, 62–76.

Bird, D.K., Schiffman, P., Elders, W.A., Williams, A.E., and McDowell, S.D. (1984) Calc-silicate mineralization of active geothermal systems. Economic Geology, 79, 671–695.

Bishop, D.G. (1972) Progressive metamorphism from prehnite-pumpellyite to greenschist facies in the Dansey Pass area, Otago, New Zealand. Geological Society of America Bulletin, 83, 3177–3198.

Chang, H.K., Mackenzie, F.T., and Schoonmaker, J. (1986) Comparisons between the diagenesis of dioctahedral and trioctahedral smectite, Brazilian offshore basins. Clays and Clay Minerals, 34, 407–423.

Cho, M., Liou, J.G., and Bird, D.K. (1988) Prograde phase relations in the State 2-14 well metasandstones, Salton Sea geothermal field, California. Journal of Geophysical Research, 93, 13081–13103.

Coombs, D.S., Nakamura, Y., and Vuagnat, M. (1976) Pumpellyite-actinolite facies schists of the Taveyanne Formation near Loeche, Valais, Switzerland. Journal of Petrology, 17, 440–471.

Ernst, W.G., Liou, J.G., and Moore, D.E. (1981) Multiple metamorphic events recorded in Tailuko amphibolites and associated rocks of the Suao-Nanao area, Taiwan. Geological Society of China Memoir, 4, 391–441.

Evarts, R.C., and Schiffman, P. (1983) Submarine hydrothermal metamorphism of the Del Puerto ophiolite, California. American Journal of Science, 283, 289–340.

Foster, M.D. (1962) Interpretation of the composition and a classification

of the chlorites. United States Geological Survey Professional Paper, 414-A, 22 p. Washington, DC.

Gottardi, G., and Galli, E. (1985) Natural zeolites, 409 p. Springer-Verlag, Berlin.

Helmold, R.P., and van der Kamp, P.C. (1984) Diagenetic mineralogy and controls on albitization and laumontite formation in Paleogene arkoses, Santa Ynez Mountains, California. American Association of Petroleum Geologists Memoir, 37, 239–276.

Hoffman, J., and Hower, J. (1979) Clay mineral assemblages as low grade metamorphic geothermometers: Application to the thrust-faulted disturbed belt of Montana, USA. Society of Economic Paleontologists and Mineralogists Special Publication, 26, 55–79.

Holdaway, M.J., Dutrow, B.L., and Hinton, R.W. (1988) Devonian and Carboniferous metamorphism in west-central Maine: The muscovite-almandine geobarometer and the staurolite problem revisited. American Mineralogist, 73, 20–47.

Horton, D.G. (1985) Mixed-layer illite/smectite as a paleotemperature indicator in the Amethyst vein system, Creed district, Colorado, USA. Contributions to Mineralogy and Petrology, 91, 171–179.

Inoue, A. (1985) Chemistry of corrensite: A trend in composition of trioctahedral chlorite/smectite during diagenesis. Journal of College of Arts and Sciences, Chiba University, B-18, 69–82.

——— (1987) Conversion of smectite to chlorite by hydrothermal and diagenetic alterations, Hokuroku Kuroko mineralization area, northeast Japan. Proceedings of International Clay Conference, Denver, 1985, 158–164.

Inoue, A., and Utada, M. (1989) Mineralogy and genesis of hydrothermal aluminous clays containing sudoite, tosudite, and rectorite in a drillhole near the Kamikita Kuroko ore deposit, northern Honshu, Japan. Clay Science, 7, 193–217.

Inoue, A., Utada, M., and Kusakabe, H. (1984a) Clay mineral composition and their exchangeable interlayer cation composition from altered rocks around the Kuroko deposits in the Matsumine-Shakanai-Matsuki area of the Hokuroku district, Japan. Journal of Clay Science Society Japan, 24, 69–77 (in Japanese).

Inoue, A., Utada, M., Nagata, H., and Watanabe, T. (1984b) Conversion of trioctahedral smectite to interstratified chlorite/smectite in Pliocene acidic pyroclastic sediments of the Ohyu district, Akita Prefecture, Japan. Clay Science, 6, 103–116,

Keith, T.E.C., and Bargar, K.E. (1988) Petrology and hydrothermal mineralogy of U.S. Geological Survey Newberry 2 drill core from Newberry caldera, Oregon. Journal of Geophysical Research, 93, 10174–10190.

Kristmannsdottir, H. (1979) Alteration of basaltic rocks by hydrothermal activity at 100–300 °C. Proceedings of International Clay Conference, Amsterdam, 1978, 359–367.

——— (1983) Chemical evidence from Icelandic Geothermal Systems as compared to submarine geothermal systems. In P.A. Rona, K. Boström, L. Laubier, and K.L. Smith, Jr., Eds., Hydrothermal processes at seafloor spreading centers, p. 291–320. NATO Conference Series IV-12, Plenum Press, New York.

Laird, J. (1988) Chlorites: Metamorphic petrology. In Mineralogical Society of America Reviews in Mineralogy, 19, 405–453.

Lang, H.M., and Rice, J.M. (1985) Geothermometry, geobarometry and T-X(Fe-Mg) relations in metapelites, Snow Peak, northern Idaho. Journal of Petrology, 26, 889–924.

Lee, M.S. (1970) Genesis of the lower ore bodies, Kaminosawa ore deposit, Kamikita mine, Aomori Prefecture, Japan. Mining Geology, 20, 378–393.

Lee, M.S., Miyajima, T., and Mizumoto, H. (1974) Geology of the Kamikita mine, Aomori Prefecture, with special reference to genesis of fragmental ores. Mining Geology Special Issue, 6, 53–66.

Liou, J.G. (1971) Stilbite-laumontite equilibrium. Contributions to Mineralogy and Petrology, 31, 171–177.

Liou, J.G., Seki, Y., Guillemette, R.N., and Sakai, H. (1985) Compositions and parageneses of secondary minerals in the Onikobe geothermal system, Japan. Chemical Geology, 49, 1–20.

McDowell, S.D., and Elders, W.A. (1980) Authigenic layer silicate minerals in borehole Elmore #1, Salton Sea geothermal field, California, USA. Contributions to Mineralogy and Petrology, 74, 293–310.

——— (1983) Allogenic layer silicate minerals in borehole Elmore #1, Salton Sea geothermal field, California. American Mineralogist, 68, 1146–1159.

Miyajima, T., and Mizumoto, H. (1965) Geology and ore deposits of the Kamikita mine, Aomori-ken. Mining Geology, 15, 142–156.

——— (1968) Geology and ore deposits of the Kamikita mine, Aomori Prefecture (2), with special reference to the volcanism and mineralization in the Okunosawa formation. Mining Geology, 18, 185–199.

MMAJ (1974) Report on regional exploration researches of Hakkoda District, 1973. Metal Mining Agency of Japan, Tokyo.

——— (1975) Report on regional exploration researches of Hakkoda District, 1974. Metal Mining Agency of Japan, Tokyo.

——— (1986) Report on regional exploration researches of Hakkoda District, 1985. Metal Mining Agency of Japan, Tokyo.

Mori, T., and Kanehira, K. (1984) X-ray energy spectrometry for electron-probe analysis. Journal of Geological Society Japan, 90, 271–285.

Newman, A.C.D., and Brown, G. (1987) The chemical constitution of clays. Chemistry of clays and clay minerals, p. 1–129. Mineralogical Society, London.

Peterson, M.N.A. (1961) Expandable chloritic clay minerals from upper Mississipian carbonate rocks of the Cumberland plateau in Tennessee. American Mineralogist, 46, 1245–1269.

Reynolds, R.C. (1980) Interstratified clay minerals. Crystal structures of clay minerals and their X-ray identification, p. 249–303. Mineralogical Society, London.

——— (1988) Mixed layer chlorite minerals. In Mineralogical Society of America Reviews in Mineralogy, 19, 601–629.

Schultz, L.G. (1963) Clay minerals in the Triassic rocks of the Colorado Plateau. United States Geological Survey Bulletin, 1147-C, 1–71.

Seki, Y., Liou, J.G., Guillemette, R., Sakai, H., Oki, Y., Hirano, T., and Onuki, H. (1983) Investigation of geothermal systems in Japan I. Onikobe geothermal area. Hydroscience and Geotechnology Laboratory Saitama University Memoir, 1, 123 p.

Shau, Y.H., Peacor, D.R., and Essene, E.J. (1990) Corrensite and mixed-layer chlorite/corrensite in metabasalt from northern Taiwan: TEM/AEM, EPMA, XRD, and optical studies. Contributions to Mineralogy and Petrology, 105, 123–142.

Środón, J., and Eberl, D.D. (1984) Illite. In Mineralogical Society of America Reviews in Mineralogy, 13, 495–544.

Tomasson, J., and Kristmannsdottir, H. (1972) High temperature alteration minerals and thermal brines, Reykjanes, Iceland. Contributions to Mineralogy and Petrology, 36, 123–134.

Velde, B. (1977) Clays and clay minerals in natural and synthetic systems, 211 p. Elsevier, Amsterdam.

Zen, E-An (1974) Prehnite- and pumpellyite-bearing mineral assemblages, west side of the Appalachian metamorphic belt, Pennsylvania to Newfoundland. Journal of Petrology, 15, 197–242.

Manuscript received April 3, 1990
Manuscript accepted December 18, 1990